arXiv:1402.5620v1 [physics.atom-ph] 23 Feb 2014

* These authors have contributed equally

Interpreting Attoclock Measurements of Tunnelling Times

Lisa Torlina*,[1] Felipe Morales*,[1] Jivesh Kaushal,[1] Harm Geert Muller,[1] Igor Ivanov,[2] Anatoli Kheifets,[2] Alejandro Zielinski,[3] Armin Scrinzi,[3] Misha Ivanov,[1,4] and Olga Smirnova[1]

[1]*Max-Born-Institut, Max-Born-Str. 2A, 12489 Berlin*

[2]*Research School of Physical Sciences, The Australian National University, Canberra ACT 0200, Australia*

[3]*Ludwig Maximilians University, Theresienstrasse 37, D-80333 Munich, Germany*

[4]*Department of Physics, Imperial College London, South Kensington Campus, SW7 2AZ London, United Kingdom*

Abstract

We discuss measurements of time-delays during strong-field ionization of atoms using few-cycle circularly polarized laser pulses – the attoclock setup. We perform numerical experiments for the benchmark system of the hydrogen atom and analyze them using fully quantum analytical theory with no ad-hoc assumptions or adjustable parameters. Excellent quantitative agreement between theory and *ab initio* simulations allows us to characterize time-delays measured by the attoclock, demonstrate that these delays are not related to tunnelling delays and are induced entirely by the interaction of the liberated electron with the long-range Coulomb potential of the ionic core. Our analysis gives access to 'ionization times' – the times when an electron exits the tunnelling barrier created by the combination of the laser field and the core potential, showing that some of the key assumptions used in the semiclassical interpretation of the attoclock experiments do not always agree with the fully quantum analysis.

Advances in attosecond technology opened up the intriguing opportunity of timing electron release during photoionization. New experimental techniques such as the attosecond streak camera [1], high harmonic spectroscopy [2], attosecond transient absorption [3] and the attoclock [4–7] are now able to provide exceptional time-resolution down to the level of tens attoseconds (1 as = 10−18 s), which is needed to time-resolve ionization. The removal of an electron from an atom or molecule by one-photon ionization creates a non-equilibrium charge distribution which evolves on the attosecond time scale [8]. Time-resolving this evolution is one of the long-standing goals of attosecond spectroscopy, and ionization time serves as a sensitive measure which encodes the dynamics of core rearrangement triggered by electron removal (see e.g. [9–11]).

While the application of intense IR fields as either pump or probe in time-resolved ionization experiments provides access to the time scale of electronic motion, it also introduces a major hurdle in interpreting such experiments [9–17]. Identifying and disentangling time-delays related to multielectron dynamics from the apparent delays induced by the interaction with the IR field is challenging both technically and conceptually. In one-photon ionization [1], understanding the nature of measured delays required accurate calibration of the attosecond streak camera, with the hydrogen atom as a benchmark [12–17].

Looking beyond one-photon ionization, several attosecond techniques are able to time-resolve multiphoton ionization in strong low-frequency fields. This process is often viewed as electron tunnelling trough the barrier created by the laser field and the core potential, thus opening the opportunity [2, 4, 5, 7] to revisit the long-standing problem of tunnelling times [18, 19]. Similar to one-photon ionization, multiphoton ionization also creates an ion in a superposition of states [20, 21] and is therefore also able to excite non-equlibrium multiectron dynamics evolving on the attosecond time scale. In contrast to one-photon ionization [9–17], there is no clear understanding of how long multiphoton ionization should take [23].

The measurement of strong-field ionization (tunnelling) times has been pioneered by the group of U. Keller [4–7], using the attoclock technique. The attoclock set-up measures photoelectron spectra produced by ionization in strong, nearly circularly polarized infrared (IR) fields. So far the interpretation of attoclock measurements has relied on an ad-hoc model, which breaks the photoionization process into two steps: (i) tunnel ionization in a quasistatic field, (ii) classical motion of the electron between the exit point from the tunnelling barrier and the detector. The accuracy of extracting time delays from attoclock

measurements within this model depends on the initial conditions assumed for the classical electron dynamics, which link the two steps but can not be established unambiguously. The accuracy of the attoclock measurements in He was challenged by a recent fully numerical study [39].

Here we provide the first fully consistent quantum-mechanical interpretation and calibration of attoclock measurements of ionization times with no ad hoc assumptions, using the combination of a fully quantum analytical theory and ab-initio simulations. To calibrate the attoclock, we use the hydrogen atom, finding excellent agreement between theory and numerical simulations. The accurate calibration of ionization delays in one-electron systems provides access to purely multielectron effects in the strong field regime, where the attoclock has revealed unexpected timing for two-electron removal [24]. We also show that for one-electron systems purely tunnelling delays during strong-field ionization are equal to zero.

I. THE ATTOCLOCK SET-UP

The tunnelling perspective on strong field ionization (Fig. 1a) provides a simple picture of how the attoclock works. The combination of a circularly polarized field and the binding potential of the atom create a rotating barrier through which an electron can tunnel (Fig.1a). Due to barrier rotation, the electron tunnels in different directions at different times and is detected at different angles after the end of the pulse (Fig.1,b,c) [25]. Nearly single-cycle circularly polarized pulses, in which the laser electric field has a single well-defined maximum, can be used to resolve the time of electron release [4–7].

In the geometry of Fig.1 (b), the field maximum is reached when the field $\mathbf{F}_L(t)$ points at the angle $\phi = 90^o$. The direction of the field maximum provides the starting time $t_0 = 0$, and attosecond rotation of the field acts as the hand of a clock [25]. The observable (Fig.1 c) is the angle- and energy resolved photoelectron spectrum, which allows one to extract the angle between the direction of the maximum electric field and the direction of the electron momentum at the peak of the photo-electron distribution.

When reading such attoclock measurements, one notes that in the absence of (i) electron-core interaction after tunnelling, and (ii) tunnelling delays, the maximum of the electron distribution is expected at the angle $\phi = 0^o$ in the geometry of Fig.1 (b,c), i.e. orthogonal

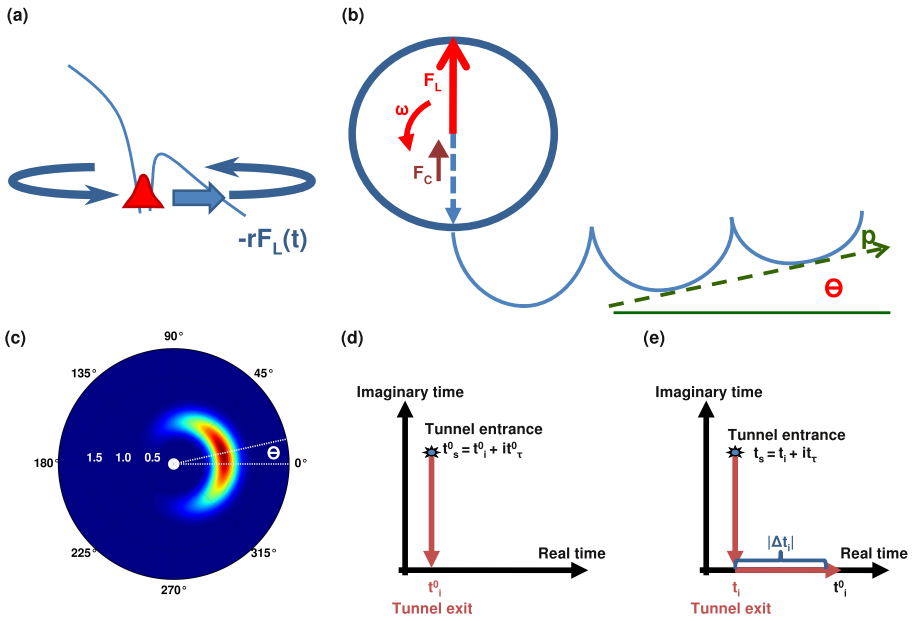

FIG. 1: The attoclock set-up. (a) Tunneling perspective on the attoclock set-up: the laser field and the core potential create a rotating barrier, through which the bound electron tunnels in different directions at different times. (b) Cartoon illustrating our geometry determined by Eq.(1). The electron which tunnels down when the laser field F_L, rotating counter-clockwise, points at $\phi = 90^o$, in the absence of the core potential will be detected at $\phi = 0^o$. The off-set θ from this angle is due to the attraction by the core potential (force F_C) and/or possible tunnelling delays. (c) Angle and energy resolved photoelectron distributions resulting from the ionization of the ground state hydrogen atom by a single cycle infrared circulary polarized pulse. Dashed lines show the attoclock observable-an off-set angle θ. (d) Saddle point solution of Eq.(8)defines the integration countour in a complex plane describing ionization in the absence of the electron-core interaction. (e) Saddle point solution of Eq.(5)defines the integration countour in a complex plane describing ionization with the electron-core interaction included.

to the peak laser field pointing at angle $\phi = 90^o$. Indeed, if the electron is released from the barrier with zero initial velocity, its final momentum $\mathbf{p}$ at the detector is given by the vector-potential $\mathbf{A}_L(t)$ of the laser field at the moment of ionization $\mathbf{p} = -\mathbf{A}_L(t)$; $\mathbf{A}_L(t)$ is orthogonal to the direction of the electric field vector $\mathbf{F}_L(t)$ for circularly polarized pulses (up to effects of the ultrashort envelope). The deviation from $\phi = 0^o$, which can come from the deflection of the outgoing electron due to attraction by the core potential (Fig.1c) and, possibly, tunnelling delays [4, 5], is characterised by the off-set angle θ, see Fig.1 (b,c). Experimentally, θ can be measured with very high accuracy ($\delta\theta \sim 2^o$) , implying remarkable precision in measuring ionization delays $\delta\tau = \delta\theta/\omega_L \sim 10$ as for 800 nm radiation used in the attoclock experiments. However, taking full advantage of this accuracy demands careful

analysis of the models and assumptions used in interpreting the attoclock measurements.

The standard assumptions are [4–7]:

- A1: exponential sensitivity of strong-field ionization to the electric field implies that there is a preferred time and direction of ionization: it is postulated that the highest probability for the electron to begin tunnelling is at the peak of the electric field.
- A2: ionization is assumed to be completed once the electron emerges from the barrier.
- A3: electron dynamics after the barrier are described classically, assuming that its point of exit (i.e. position) and the distribution of initial velocities (typically assumed to be a Gaussian centred around zero) are known [7]. More advanced approaches involve classical Monte-Carlo-type simulations [22], and may include the additional capability of treating non-adiabatic effects during tunnelling [26].

We present a consistent, fully quantum, analytical treatment which shows excellent quantitative agreement with *ab initio* simulations for the hydrogen atom. Importantly, it includes the concept of trajectories, allowing us to assess the accuracy of assumptions **A1-A3** while interpreting the attoclock measurements. We show that, in contrast to assumption **A3**, trajectories are never fully classical: while the measured quantity (electron momentum) is real, the trajectories retain an imaginary component of the coordinate all the way to the detector. This property is directly related to the fact that, in a long-range potential, ionization is not yet completed at the moment when the electron exits the tunnelling barrier, in contrast to assumption **A2**. Ongoing ionization leads to a further re-shaping of the outgoing wavepacket after the tunnelling step is formally completed. As a result of this reshaping, we find that the dominant contribution to the photo-electron spectrum may come from ionization that occurs before the maximum of the electric field, in contrast to assumption **A1**.

II. ANALYTICAL APPROACH

Our quantum formalism is based on the time-dependent analytical R-matrix approach (ARM) [27–30], which yields a consistent time-domain analytical theory of strong-field ionization for arbitrary core potentials. In the spirit of the R-matrix approach, the configuration space is split into two regions: an inner region enclosing an atom or a molecule and an outer

region, remote from the singularity of the core. In the outer region, propagators based on the eikonal-Volkov (EVA) states [31] are accurate. The matching of inner region solutions to outer-region EVA states occurs at the R-matrix boundary and is achieved using the Bloch operator, as in the standard R-matrix approach.

We define the laser field $\mathbf{F}_L(t) = -\partial \mathbf{A}_L(t)/\partial t$ via the vector-potential $\mathbf{A}_L(t)$:

$$\mathbf{A}_L(t) = -A_0 f(t)(\cos(\omega t)\ \hat{\mathbf{x}} + \sin(\omega t)\ \hat{\mathbf{y}}), \tag{1}$$

where $f(t)$ is the pulse envelope and ω is the carrier frequency. The field rotates counter-clockwise and points at 90^o when reaching its maximum at $t = 0$. We consider ionization from the ground state of the hydrogen atom, to benchmark it against ab-initio calculations. The photoelectron spectrum $|a_{\mathbf{p}}(T)|^2 \propto |\ e^{-iS(T,\mathbf{p})}|^2$ at the observation time T is determined by the action $S = \mathrm{Re}S + i\mathrm{Im}S$ along the quantum trajectory specified below, where $\mathbf{p}$ is the electron momentum at the detector [29, 30]. The action $S = S_{SFA} + W_C$ includes the component S_{SFA} accumulated by the electron in the laser field and the component W_C accumulated due to the interaction with the core potential. The full expression is [30],

$$|a_{\mathbf{p}}(T)|^2 = |R_{\kappa lm}(\mathbf{p})|^2\ e^{2\mathrm{Im}W_C(T,\mathbf{p})}\ e^{2\mathrm{Im}S_{SFA}(T,\mathbf{p})}. \tag{2}$$

where $R_{\kappa lm}(\mathbf{p})$ encodes the angular structure of the initial state. For the spherically symmetric ground s-state of the hydrogen atom, it does not impact the angle-resolved spectra. The second term in Eq.(2) involves the contribution to the action accumulated due to the interaction between the departing electron and the core:

$$W_C(T, \mathbf{p}, t_s) = \int_{t_s - i\kappa^{-2}}^{T} dt\ U(\mathbf{r}_s(\mathbf{p}, t, t_s)), \tag{3}$$

where $U(\mathbf{r}_s)$ is the core potential of the atom or molecule evaluated along the laser-driven trajectory of the departing electron,

$$\mathbf{r}_s(\mathbf{p}, t, t_s) = \int_{t_s}^{t} dt'\ (\mathbf{p} + \mathbf{A}(t')), \tag{4}$$

and $t_s = t_i + it_\tau$ denotes the complex solution to the saddle point equation:

$$\partial S_V(T, \mathbf{p}, t_s)/\partial t_s + \partial W_C(T, \mathbf{p}, t_s)/\partial t_s = I_p, \tag{5}$$

where I_p is the ionization potential and κ in Eq. (3) is $\kappa = \sqrt{2I_p}$. In Eq.(5), $S_V(T, \mathbf{p})$ is the action accumulated by the electron in the laser field only:

$$S_{SFA} = S_V - I_p t_s, \tag{6}$$

$$S_V(T, \mathbf{p}, t_s) = \frac{1}{2}\int_{t_s}^{T} [\mathbf{p} + \mathbf{A}(t)]^2 dt \quad . \tag{7}$$

The last term in Eq.(2) $e^{2\mathrm{Im}S_{SFA}}$ would have been the standard exponential factor in the analytical treatment of strong-field ionization if t_s were substituted by t_s^0 – the solution of the saddle point equation which does not include the electron-core interaction (the strong field approximation, SFA):

$$\partial S_V(T, \mathbf{p}, t_s^0)/\partial t_s^0 = I_p. \tag{8}$$

In the absence of electron-core interaction, the real part t_i^0 of the saddle point solution t_s^0 has clear meaning. It corresponds to the so-called ionization time, since for all times $t > t_i^0$ the photoelectron spectrum $|a_{\mathbf{p}}^0(t)|^2 \propto e^{2\mathrm{Im}S_{SFA}(t,\mathbf{p},t_s^0)}$ and the ionization probability $\int |a_{\mathbf{p}}^0(t)|^2 d\mathbf{p}$ do not change any more: ionization is completed by time t_i^0. Indeed, the imaginary component of the action $S_{SFA}(t, \mathbf{p}, t_s^0)$ is only accumulated while integrating in Eq.(7) from t_s^0 to t_i^0 following the arrow in Fig.1(d). The same property of the integral in Eq.(7) has prompted the tunnelling perspective, where tunnelling corresponds to motion in imaginary time from $\mathrm{Im}t_s^0$ to zero, and $\mathrm{Re}t_s^0 = t_i^0$ corresponds to the exit time, the time when the electron leaves the tunnelling barrier. Within this approach, in the absence of electron-core interaction, tunnelling from the bound state is instantaneous: it starts and finishes at the same real time t_i^0 (Fig.1(d)) and ionization time directly maps into the electron detection angle ϕ (see e.g. [32, 33]):

$$\omega t_i^0 = \phi + \phi^{env}. \tag{9}$$

Here ϕ^{env} is a small correction to the standard mapping $\omega t_i^0 = \phi$ due to the rapidly changing envelope of the single cycle pulse; Eq. (9) is the real part of the exact solution of Eq. (8). Thus, the electron detection angle measures the time when ionization was completed.

We will revisit the question about possible tunnelling delays later, when comparing these theoretical results with the ab-initio simulations.

The presence of the time derivative $\partial W_C(T, \mathbf{p}, t_s)/\partial t_s$ of the action W_C associated with the electron-core interaction in Eq.(5) shifts the unperturbed saddle point t_s^0 by Δt_s: $t_s = t_s^0 + \Delta t_s$. The real part $\Delta t_i = \mathrm{Re}\Delta t_s$ of the correction Δt_s defines the 'ionization delay' for the long-range electron-core interaction (Fig.1(e)), relative to the case of the short-range potential [23]. Seeking a solution of the saddle point equation (5) of the form,

$$t_s = t_s^0 + \Delta t_s, \tag{10}$$

expanding Eq.(5) in a Taylor series around t_s^0, and keeping all terms up to first order in the electron-core interaction, we obtain the Coulomb correction to the saddle point time Δt_s:

$$\Delta t_s = -\frac{\partial W_C(T, \mathbf{p}, t_s^0)}{\partial t_s^0} \left(\frac{\partial^2 S_V(T, \mathbf{p}, t_s)}{\partial t_s^2} \right)^{-1}. \tag{11}$$

Taking into account that the saddle point equation (8) establishes a functional dependence $t_s^0(I_p)$ and differentiating both parts of Eq.(8) wrt t_s^0, we obtain:

$$\left(\frac{\partial^2 S_V(T, \mathbf{p}, t_s)}{\partial t_s^{02}} \right)^{-1} = \frac{dt_s^0}{dI_p}. \tag{12}$$

Combining Eqs.(11,12), we obtain:

$$\Delta t_s = -\frac{\partial W_C(T, \mathbf{p}, t_s^0)}{\partial t_s^0} \frac{dt_s^0}{dI_p}. \tag{13}$$

A practical way of calculating Δt_s is to recall that $W_C(T, \mathbf{p}, t_s^0)$ implicitly depends on I_p only via $\kappa(I_p)$ and $t_s(I_p)$:

$$\frac{dW_C(T, \mathbf{p}, t_s^0)}{dI_p} = \frac{\partial W_C(T, \mathbf{p}, t_s^0)}{\partial t_s^0} \frac{dt_s^0}{dI_p} + \frac{\partial W_C(T, \mathbf{p}, t_s^0)}{\partial \kappa} \frac{d\kappa}{dI_p}. \tag{14}$$

Thus, one obtains Δt_s Eq.(13) by evaluating the full derivative of W_C in Eq. (3) wrt I_p keeping the parameter κ in the lower limit of the integral in Eq. (3) constant:

$$\Delta t_s = -\frac{dW_C(T, \mathbf{p}, t_s^0)}{dI_p}|_{\kappa = const}. \tag{15}$$

The constraint in Eq.(15) is only important for calculating the imaginary part of the time Δt_s, since the the real part of W_C,

$$\mathrm{Re}[W_C] = \int_{t_i^0}^{T} dt \mathrm{Re}[\ U(\mathbf{r}_s(\mathbf{p}, t, t_s^0))] \tag{16}$$

does not depend on κ explicitly. The expression for the Coulomb correction to the real ionization time becomes straightforward:

$$\Delta t_i = -\frac{d\mathrm{Re}[W_C(T, \mathbf{p}, t_s^0)]}{dI_p}. \tag{17}$$

The angle and energy resolved photo-electron spectra are calculated usingq equations (2,3,6,7) with t_s defined via Eqs.(8,10,17).

III. RESULTS

Fig.2 compares the angle and energy resolved photo-electron spectra calculated analytically with those obtained by solving the time-dependent Schrödinger equation numerically for the H atom interacting with a circularly polarized single-cycle laser pulse Eq.(1) with the envelope

$$f(t) = \cos^4(\omega t/4). \tag{18}$$

The details of the numerical approaches are described in the Methods section. The contours in Fig.2 correspond to signal intensity changing from 0.1 to 0.9, in steps of 0.1. The analytical results (solid contours) are in very good agreement with the numerical results (dashed contours). The off-set angle θ is extracted from the peak position of the angle and energy resolved photoelectron distribution, which specifies $\mathbf{p}_{max} = (p_r \cos\phi_{max}, p_r \sin\phi_{max})$, where ϕ_{max} and p_r are the peak angle and radial momentum (Fig.2). In our geometry (Fig.1(c)), $\theta = \phi_{max}$. Fig.3(a) shows the off-set angle θ as a function of laser intensity. We present three sets of numerical calculations which use three different methods and propagation algorithms for solving the TDSE, see Methods section. The agreement between numerical results is very good, with the deviation not exceeding 2^o. The deviation between analytical and numerical results is also within $\delta\theta \simeq 2^o$.

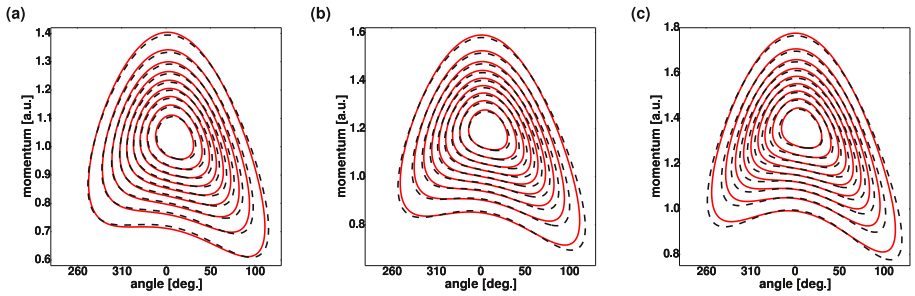

FIG. 2: Angle and energy resolved photoelectron spectra produced by strong field ionization of Hydrogen atom for different intensities. The laser pulse is specified in Eqs.(1,18). The contours correspond to signal intensity changing from 0.1 to 0.9, in steps of 0.1, with the inner-most contour at 0.9. Solid contours correspond to analytical results, dashed to numerical results for $\lambda = 800$ nm and intensities: (a) I=1.75 10^{14} W/cm^2, (b) I=2.5 10^{14} W/cm^2, (c) I=3.4 10^{14} W/cm^2.

This deviation is analysed further in Fig.3(b), where we zoom into the region of intensities $I = 1 - 3 \times 10^{14}$W/cm^2 and we see a small discrepancy between the analytical (red squares) and numerical (blue circles) results. The error-bars highlight the extremely flat nature of the distribution around the maximum, even for the single-cycle pulse that we have used. In particular, the error-bars indicate the angle at which the distribution falls by only 0.1% compared to the peak of signal intensity. Within 0.1% of the peak of the distribution, the analytical and numerical off-set angles agree. This flatness of the spectrum may also challenge the accuracy of identifying θ in experiments, given the ever-present signal-to-noise ratio.

All calculations show a very interesting intensity trend. At lower intensities, when the barrier for tunnelling is thicker, there is a bigger deflection angle. Does this trend represent a tunnelling delay, as suggested recently [26, 34]? In the hydrogen atom, the angular offset may come from two sources: tunnelling delay and electron-nucleus interaction. Both theoretically and numerically, we can turn off the electron-nucleus interaction after tunnelling by replacing the Coulomb potential with the short-range Yukawa potential $U_Y = Ze^{-r/a}/r$, where $Z = 1.94$ and $a = 1.0$a.u. were chosen to yield the ionization potential of the H-atom. At the same time, the tunnelling barrier formed by the laser field and the short-range Yukawa potential is still present. The results of these calculations are summarized in Fig.3 (a) and Fig.4. In all cases, the deviation angle is equal to zero: the attoclock measures no tunnelling delay for the short-range potential $U_Y = Ze^{-r/a}/r$, in agreement with theory. Thus, for the H-atom, the offset angle θ is determined by the interaction of the outgoing electron, driven

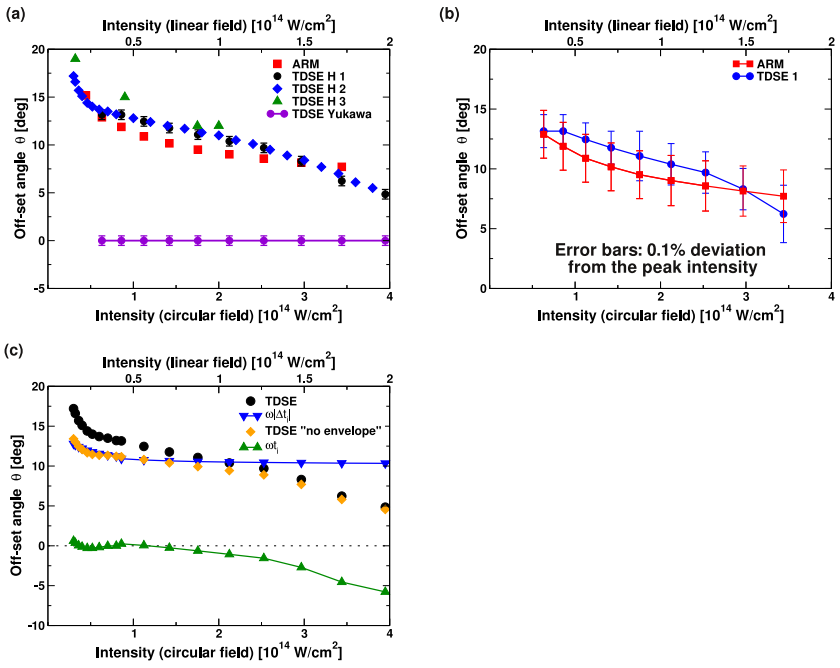

FIG. 3: The off-set angle θ extracted from the electron spectra. (a) Analytical (red squares) and numerical off-set angles. Three independent numerical algorithms have been used, described in [43], [38], and [39]. The corresponding results are labelled 'TDSE H 1' [38], black circles, 'TDSE H 2' based on the t-SURFF method [37] blue diamonds, 'TDSE H 3' [39] green triangles. Violet circles show off-set angles for the Yukawa potential. (b) Analytical (red squares) and numerical (blue circles, TDSE H 1) results for the off-set angle. The error-bars include angles lying within only 0.1 % deviation from the peak of the signal intensity. (c) Reading the ionization time from the attoclock observable θ. The attoclock observable (black circles, TDSE H 1 and TDSE H 2) provides access to the ionization time $t_i = \mathrm{Re}t_s$ (green triangles) by subtracting the ionization delay Δt_i (blue inverted triangles) calculated for $\mathbf{p}_{max}$ obtained numerically from the ab-initio results corrected for the effects of the ultra-short envelope (orange diamonds).

by the laser field, with the core potential, and not by tunnelling delays. We can now use our analytical theory to analyse the underlying physics.

Using Eqs.(9-10) and taking into account that $\Delta t_i < 0$, we can connect the real part of the saddle point in Eq.(10) to the attoclock observable θ:

$$\mathrm{Re}\omega t_s = \omega t_i = \theta + \phi^{env} - \omega|\Delta t_i|. \tag{19}$$

The black circles in Fig. 3(c) show the results of the TDSE calculation (combined sets of TDSE H 1 and TDSE H 2) for the off-set angle θ for hydrogen atom. Orange diamonds show $\theta + \phi^{env}(\mathbf{p}_{max})$ ($\phi^{env} < 0$, $\phi^{env}(\mathbf{p}_{max})$ is calculated for $\mathbf{p}_{max}$ obtained numerically) removing the effects of the ultrashort envelope from the TDSE results. We have verified that, within

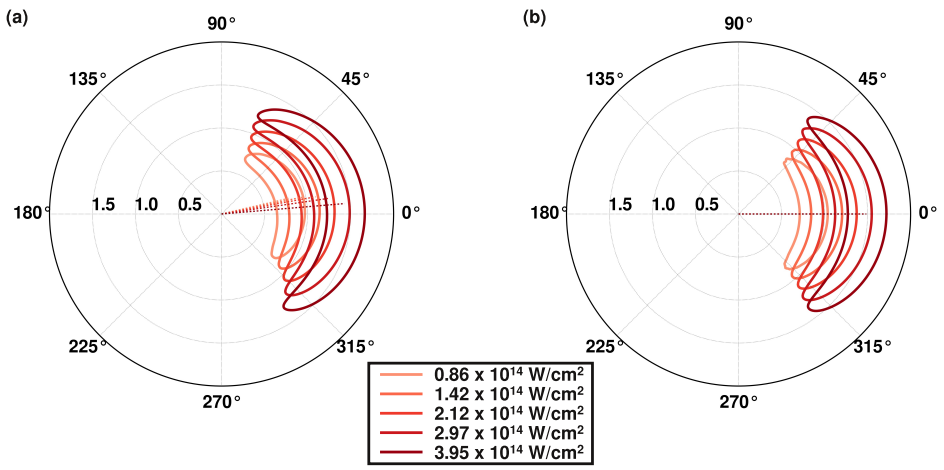

FIG. 4: Attoclock measures no tunneling delays for the Yukawa potential. Contours of angle and energy resolved photoelectron spectra for the Coulomb (a) and Yukawa (b) potential, for different intensities. Each contour corresponds to the same signal strength, but different laser intensity. The pulse duration and wavelength are as in Figs.2,3.

the analytical approach, off-set angles corrected in this way become virtually independent of the pulse envelope. Fig. 3(c) shows that for intensities $I \leq 2\times10^{14}\mathrm{W/cm^2}$, the envelope-free offset angle (orange diamonds) coincides with the ionization delay $\omega|\Delta t_i(\mathbf{p}_{max})|$ ($\Delta t_i(\mathbf{p}_{max})$ is calculated for $\mathbf{p}_{max}$ obtained numerically), yielding ionization times $\omega t_i \simeq 0$, shown with green triangles in Fig. 3(c). Thus, at these intensities, the majority of electrons are indeed born at the peak of the field. At higher intensities, however, ionization times become negative, signifying that ionization begins before the peak of the field, for the parameters of the numerical experiment. The saturation of ionization could hardly be responsible for this surprising result, since the ionization probability remains very small. The barrier suppression limit for tunnelling in DC electric field is also not yet reached. How can we understand this result using the language of quantum trajectories $\mathbf{r}_s(\mathbf{p}, t, t_s)$ Eq.(4)?

Each trajectory is characterized by its final momentum $\mathbf{p}$. It starts at a complex ionization time t_s and the coordinate $\mathbf{r}_s(\mathbf{p}, t, t_s)$ is, in general, complex. The interaction with the core potential along such trajectory also acquires a complex component, maintaining it even after the electron 'exits the tunnelling barrier' at t_i. Consequently, the contribution to the action associated with the Coulomb interaction $\exp(-iW_C)$ is not only a phase – it also changes the trajectory amplitude. The physics is simple: in the long-range Coulomb potential, the ionization process is not completed at the exit point from the barrier t_i [30], and this contributes to the reshaping of the electron wave-packet as it moves towards the detector.

This reshaping of the electron wave-packet shifts $\mathbf{p}_{max}$ across the spectrum and modifies the direction in which the majority of electrons will be detected. It can also shift the ionization time $t_i(\mathbf{p}_{max})$ from $t_0 = 0$.

To summarize, the electron core interaction plays a dual role: it is responsible for the ionization delay $\Delta t_i(\mathbf{p})$ along each individual trajectory as well as the deviation of the ionization time $t_i(\mathbf{p}_{max})$ from the peak of the laser field due to the continuing ionization process, which changes the population of each trajectory even after the exit from the tunnelling barrier. The reshaping of the wave-packet may imply the breakdown of the key assumptions used for interpreting the attoclock measurements: that ionization is completed when the electron emerges from the tunnelling barrier, and that the majority of electrons start tunnelling at the peak of the field.

We have provided robust self-consistent procedure for calibrating the attoclock. Ionization times reconstructed from numerical experiment do not correspond to positive delays with respect to the peak of the field. The reconstruction reveals that for low intensity ionization occurs at the peak of the field. As intensity increases ionization begins before the peak of the field. This picture leaves no room for tunnelling delays in strong field ionization of the hydrogen atom.

IV. OUTLOOK

Exit times t_i have been measured recently using the high harmonic generation (HHG) set-up [2]. Such measurements are not equivalent to the attoclock, since the electron trajectories relevant for HHG are different from those relevant for the attoclock. The latter end up at the detector, while the former return to the core and recombine. In particular, in the HHG set-up, delays associated with the deceleration of the departing electron by the Coulomb potential are to some extent compensated by the subsequent acceleration in the Coulomb potential during the electron's return.

The attoclock provides well defined, robust and accurate measurement of the the full ionization time $\mathrm{Re}t_s + |\Delta t_i(\mathbf{p}_{max})|$, but not of the 'exit' time t_i and the ionization 'delay' $|\Delta t_i(\mathbf{p}_{max})|$ [23] separately. Our analytical theory provides simple and accurate expression for $|\Delta t_i(\mathbf{p}_{max})|$, with no ad-hoc assumptions. While both t_i and $|\Delta t_i(\mathbf{p}_{max})|$ encode the interaction of the outgoing electron with the core, conceptually they provide different infor-

mation on the ionization process. The deviation of the 'exit' time t_i from the peak of the field reflects the continuing re-shaping of the electronic wavepacket after tunnelling [44]. In the conventional tunnelling problem of a wavepacket incident on a potential barrier, wavepacket reshaping during tunnelling is known to yield negative delays when one follows the motion of the wavepacket peak before and after the barrier. We show that, within our analytical theory, the negative delays ($t_i(\mathbf{p}_{max}) < t_0 = 0$) in Fig.3(c) (green curve) for the specific example of the hydrogen atom and the single-cycle 800 nm pulse studied here have the same origin: reshaping of the electron wave-packet during ionization.

In one-photon ionization, the accurate calibration of time-delays for the hydrogen atom allows one to access delays associated with multi-electron effects and core rearrangement [13, 15, 35, 40]. The same applies to multi-photon ionization time-resolved by the attoclock: the ability to analytically and accurately calibrate ionization delays $\Delta t_i(\mathbf{p})$ in the benchmark system opens the opportunity to identify non-trivial contributions associated with multi-electron effects, be it the effects of the self-consistent field [7, 41] or genuine multi-electron correlation.

For one-electron systems, purely tunnelling delays are absent. However, extending this conclusion to multi-electron systems is not substantiated. On the contrary, purely mathematical considerations suggest that core rearangment due to electron-electron correlation during the tunnelling process may, in principle, introduce time-delays inside the classically forbidden region.

Indeed, from the mathematical perspective, the absence of pure 'tunneling' delays during strong-field ionization follows from the saddle-point analysis of the quantum-mechanical integrals describing the ionization process. As long as the integral can be performed along the contours shown in Fig.1(d,e), moving vertically from the complex-valued saddle point to the real time axis, purely 'tunnelling' delays between t_s and $t_i = \mathrm{Re}t_s$ are formally absent. However, the quantum trajectory $\mathbf{r}$ becomes complex-valued along this contour, and so does the interaction potential. For a purely Coulomb potential $U(\mathbf{r}) = 1/r$ and circular polarization, the analytical continuation in the complex plane does not lead to problems for the dominant trajectories. This does not apply, however, to the electron-electron correlation potential $U_{ee} = 1/|\mathbf{r} - \mathbf{r}'|$: the analytical continuation to complex-valued $\mathbf{r}$ for arbitrary $\mathbf{r}'$ is by no means trivial [42]. The simple contour shown in Fig.1(e) may be forced to go around branch cuts associated with the correlation interaction on the complex plane.

Physically, this mathematical property will imply the presence of genuine time-delays due to correlation-driven transitions in the ionic core during multi-photon ionization – an important new channel in tunnel ionization from multi-electron systems [28, 36]. Correlation-induced delay is the key contributor to time-delays in one-photon ionization [9–11, 16], and is likely to play a similar role in multi-photon ionization. The key role of the accurate analytical calibration of the attoclock derived here is the ability to access these times, removing the more straightforward single-particle contributions.

V. METHODS

Our numerical simulations have used three different algorithms to produce ab-initio spectra of strong-field ionization induced by a single-cycle 800 nm laser pulse. The data labeled 'TDSE H 1' (F. Morales and H. G. Muller) have used the numerical procedure and the code described in detail in [38]. The data labeled 'TDSE H 2' (A. Zielinski and A. Scrinzi) were obtained using the t-SURFF method described in [43]. The data labelled 'TDSE H 3' (I. Ivanov and A. Kheifets) have used the numerical procedure and the code described in detail in [39].

The method used for the calculations labeled 'TDSE H 1' (F. Morales and H. G. Muller) has been monitored for convergence by changing the maximum angular momentum up to $L_{max} = 120$, while the radial grid size was increased up to r_{max}=2700 a.u. The spectrum was obtained by projection on the exact field-free continuum states of the H-atom after the end of the laser pulse. The step size of radial grid was δr=0.15 a.u. and the time-step was δt=0.05 a.u. Convergence was monitored by varying δr down to 0.05 a.u. and the time-step δt down to 0.04 a.u.

T-SURFF ('TDSE H 2', A. Zielinski and A. Scrinzi) combines a numerical solution in an inner region with an approximate analytical solution in terms of Volkov states outside. The method is efficient, as the numerical part of the solution can be kept comparatively small: converged results were obtained with an inner region $|\vec{r}| < r_{\max} = 120$ a.u. using a finite-element radial discretization with 310 coefficients and an expansion into spherical harmonics up to $L_{\max} = 95$. The dominant error in the offset-angle θ arises from the absence of electron-ion interaction in the Volkov states. It is $\lesssim 0.3^\circ$ at the lowest intensities and drops to below $< 0.01^\circ$ for intensities $> 10^{14}$ W/cm^2. A detailed description of method and

code, as well as numerical examples can be found in [37, 43].

The method used for the calculations labeled 'TDSE H 3' (I. Ivanov and A. Kheifets) has been monitored for convergence by changing the maximum angular momentum up to $L_{max} = 80$, while the radial grid size was increased up to r_{max}=300 a.u. for calculations in the length and the velocity gauge (fully agreed between themselves). The spectrum was obtained by projection onto the exact field-free continuum states of the H-atom after the end of the laser pulse. The step size of radial grid was δr=0.1 a.u. and the time-step was δt=0.01 a.u.. Convergence was monitored by varying δr down to 0.05 a.u. and the time-step δt down to 0.005 a.u..

[1] Schultze, M. et al. Delay in photoemission. Science 328, 16581662 (2010).

[2] Shafir, D. et al. Resolving the time when an electron exits a tunnelling barrier, Nature 485 (7398), 343-346 (2012)

[3] Goulielmakis, E. et al, Real-time observation of valence electron motion, Nature 466 (7307), 700-702 (2010)

[4] Eckle, P. et al. Attosecond ionization and tunneling delay time measurements in helium. Science 322, 1525-1529 (2008)

[5] Eckle, P. et al. Attosecond angular streaking, Nature Physics 4, 565-570 (2008).

[6] A. N. Pfeiffer, C. Cirelli, M. Smolarski, R. Dörner, U. Keller Timing the release in sequential double ionization,Nature Physics, vol. 7, pp. 428-433, 2011

[7] A. P. Pfeiffer et al, Attoclock reveals natural coordinates of the laser-induced tunnelling current flow in atoms, Nature Physics 8, 7680 (2012)

[8] Breidbach, J. Cederbaum, L. S., Universal Attosecond Response to the Removal of an Electron, Phys. Rev. Lett. 94, 033901 (1-4) (2005)

[9] S Sukiasyan, KL Ishikawa, M Ivanov, Attosecond cascades and time delays in one-electron photoionization, Physical Review A 86 (3), 033423 (2012)

[10] A. S. Kheifets and I. A. Ivanov, Phys. Rev. Lett. 105, 233002 (2010).

[11] L. R. Moore, M. A. Lysaght, J. S. Parker, H. W. van der Hart, and K. T. Taylor, Phys. Rev. A 84, 061404 (2011).

[12] Klunder, K. et al. Probing Single-Photon Ionization on the Attosecond Time Scale, Phys.

Rev. Lett. 106, 143002 (1-4) (2011)

[13] M. Ivanov, O. Smirnova How accurate is the attosecond streak camera? Phys. Rev. Lett, 107 (21), 213605

[14] S Nagele et al, Time-resolved photoemission by attosecond streaking: extraction of time information, J. Phys. B: At. Mol. Opt. Phys. 44 081001 (2011)

[15] R. Pazourek, S. Nagele and J. Burgdorfer. Time-resolved photoemission on the attosecond scale: opportunities and cahallenges. Faraday Discuss. 163, 353 (2013)

[16] JM Dahlström, A LHuillier, A Maquet, Introduction to attosecond delays in photoionization Journal of Physics B: Atomic, Molecular and Optical Physics 45 (18), 183001 (2012)

[17] J.M. Dahlström, et al Theory of attosecond delays in laser-assisted photoionization Chemical Physics Volume 414, 5364 (2013)

[18] Landauer, R. Martin, Th. Barrier interaction time in tunneling. Rev. Mod. Phys. 66, 217228 (1994).

[19] E. H. Hauge and J. A. Stølvneng, Tunneling times: a critical review, Reviews of Modern Physics, 61, 917-936, (1989)

[20] O. Smirnova et al, High harmonic interferometry of multi-electron dynamics in molecules, Nature 460 (7258), 972-977, (2009)

[21] A. E. Boguslavskiy, et al The multielectron ionization dynamics underlying attosecond strong-field spectroscopies Science 335 (6074), 1336-1340, (2012)

[22] SP Goreslavski, GG Paulus, SV Popruzhenko, NI Shvetsov-Shilovski Coulomb asymmetry in above-threshold ionization, Phys. Rev. Lett. 93 (23), 233002, (2004)

[23] Olga Smirnova, Jivesh Kaushal, Lisa Torlina, Felipe Morales, Misha Ivanov, Spin-orbit Larmor clock for ionization, in preparation.

[24] A. N. Pfeiffer, C. Cirelli, M. Smolarski, X. Wang, J. H. Eberly, R. Dörner, U. Keller, Breakdown of the independent electron approximation in sequential double ionization, New J. Phys. 13, 093008 (2011)

[25] Adrian N. Pfeiffer, Claudio Cirelli, Mathias Smolarski, Ursula Keller, Recent attoclock measurements of strong field ionization, Chemical Physics Volume 414, 39 (2013)

[26] R. Boge, C. Cirelli, A. S. Landsman, S. Heuser, A. Ludwig, J. Maurer, M. Weger, L. Gallmann, and U. Keller. Probing Nonadiabatic Effects in Strong-Field Tunnel Ionization, PRL 111, 103003 (2013)

[27] Torlina, L., Smirnova, O. Time-dependent analytical R-matrix approach for strong-field dynamics. I. One-electron systems, Physical Review A 86 (4), 043408 (1-13) (2012)

[28] Torlina, L., et al., Time-dependent analytical R-matrix approach for strong-field dynamics. II. Many-electron systems, Physical Review A 86 (4), 043409 (1-12) (2012)

[29] J Kaushal, O Smirnova Nonadiabatic Coulomb effects in strong-field ionization in circularly polarized laser fields, Physical Review A 88 (1), 013421, (2013)

[30] L Torlina, J Kaushal, O Smirnova, Time-resolving electron-core dynamics during strong-field ionization in circularly polarized fields, Physical Review A 88 (5), 053403, (2013)

[31] O Smirnova, M Spanner, M Ivanov, Analytical solutions for strong field-driven atomic and molecular one-and two-electron continua and applications to strong-field problems Physical Review A 77 (3), 033407, (2008)

[32] Barth, I., and Smirnova, O., Nonadiabatic tunneling in circularly polarized laser fields: Physical picture and calculations, Physical Review A 84 (6), 063415 (1-5) (2011)

[33] I Barth, O Smirnova, Nonadiabatic tunneling in circularly polarized laser fields. II. Derivation of formulas Physical Review A 87 (1), 013433 (2013)

[34] A. Landsman et al, http://arxiv.org/pdf/1301.2766.pdf

[35] T Carette, JM Dahlström, L Argenti, E Lindroth, Multiconfigurational Hartree-Fock close-coupling ansatz: Application to the argon photoionization cross section and delays Physical Review A 87 (2), 023420 (2013)

[36] Z. Walters and O. Smirnova, Attosecond correlation dynamics during electron tunnelling from molecules, Journal of Physics B: Atomic, Molecular and Optical Physics, v 43, 161002, (2010)

[37] A. Scrinzi, t-SURFF: fully differential two-electron photo-emission spectra New Journal of Physics 14, 085008 (2012)

[38] Muller, H. G. An efficient propagation scheme for the time-dependent Schrödinger equation in the velocity gauge. Laser Physics 9 (1999): 138-148.

[39] I. Ivanov, A. Kheifets, Strong-field ionization of He by elliptically polarized light in attoclock configuration. Physical Review A 89 (2), 021402 (2014)

[40] A. S. Kheifets, Time delay in valence shell photoionization of noble gas atoms, Phys. Rev. A 87, 063404 (2013)

[41] N. I. Shvetsov-Shilovski, D. Dimitrovski, and L. B. Madsen, Ionization in elliptically polarized pulses: Multielectron polarization effects and asymmetry of photoelectron momentum

distributions, Physical Review A 85, 023428 (2012)

[42] Nimrod Moiseev, Nonhermition quantum mechanics, Cambridge University Press, 2011

[43] Tao, Liang and Scrinzi, Armin, Photo-electron momentum spectra from minimal volumes: the time-dependent surface flux method, New Journal of Physics, 14, 013021.

[44] In addition to the deformation of the wavepacket, its norm continues to change (see [30]).